Efficient heat removal via thorny devil nanofiber, silver nanowire, and graphene nanotextured surfaces

Hyun Yoon[a, †], Min-woo Kim[a, †], Hayong Kim[a, †], Do-Yeon Kim[a], Seongpil An[a], Jong-Gun Lee[a], Bhavana N. Joshi[a] , Hong Seok Jo[a], Jeehoon Choi[c], Salem S. Al-Deyab[d], Alexander L. Yarin[a,e*], Sam S. Yoon[a,*]

[a]School of Mechanical Engineering, Korea University, Seoul, Korea

[b]Green School, Korea University, Seoul, 136-713, Republic of Korea

[c]LG Electronics Inc, Seoul, Korea.

[d]Petrochemicals Research Chair, Dept. of Chem., King Saud University, Riyadh 11451, Saudi Arabia

[e]Department of Mechanical and Industrial Engineering, University of Illinois at Chicago, 842 West Taylor Street, Chicago, Illinois 60607-7022, United States

Abstract

Several types of nano-textured surfaces were studied with the goal to enhance heat removal rate in a cooling device (a heat sink) with water flow-through. The nano-textured surfaces where heat removal to flowing water took place included: (i) electrospun copper-plated thorny-devil nanofibers deposited on the copper substrate, (ii) graphene oxide flakes sprayed on the copper substrate, and (iii) silver nanowires spin-coated on a separate copper substrate. There cooling performance was monitored by measuring the difference between the outlet and inlet temperature of water flowing through the heat sink and the temperature of the nano-textured copper substrate in the heat sink. The effect of the macroscopic vortex generator (wires) on cooling of the heat sink surface was less than that of the nano-textured surfaces, which revealed that the latter provide a much larger interfacial area, rather than an extra flow mixing, to enhance heat transfer rate. Of the nano-textured surfaces the most significant cooling enhancement was achieved with silver nanowires.

Keywords: Water cooling, Heat removal, Nanotextured surface, Nanomaterials

[†]These authors have contributed equally

*Corresponding author: skyoon@korea.ac.kr, ayarin@uic.edu

1. Introduction

Nano-textured surfaces having at least one dimension in the nanometer range are in high demand in various applications such as electronics, photonics, advanced materials and biomedical[1-3]. Such nano-textured surfaces also hold great promise for electronic cooling due to their superior heat transfer properties[4-11] Different micro/nano-textured materials were either synthesized or formed by deposition techniques having in mind enhanced cooling of high-heat-flux surfaces[12-14]. These micro/nano-textured materials and devices can provide efficient cooling systems for the miniaturized electronics, such as multicore processors, lasers, radars, lighting equipment, and power electronics by dissipating heat flux efficiently and thus, minimizing the malfunction probability or even failure of the devices.[13] However, removing heat has been a great challenge in the field of electronics cooling because it is essentially limited by the surface area and coolant types, which is difficult to modify.[15, 16] A space to which a cooling device is employed in electronics is in general extremely confined. Power consumption should be minimized for energy saving reason and to minimize acoustic noise driven by pumps or fans at higher convective heat transfer. Nano-texturing can provide an alternative route to meet the desired goal under these challenges. Nano-texturing can also facilitate enhanced cooling via, first, the increased surface areas and, second, by generating numerous small-scale structures that promote an extra mixing.

In general, water or air have been used as coolants because of their facile availability. In the case of water cooling, hydrophobic rough surfaces can transfer heat faster by inducing faster boiling.[17] . References[12],[17] reported use of scratched silicon and nanowire arrays of silicon and copper for their boiling studies. The use of such textured substrates has increased the heat transfer by creating more active sites for boiling. The authors of Ref.[13] deposited different

ZnO nano-structures on copper, aluminium and silicon substrates for a micro-reactor for faster cooling of a heated device. They have observed a ten-fold increase in heat transfer rate as compared to the bare substrate case in forced convection. Copper-plated electrospun nanofibers (thorny-devil nanofibers) were used in drop/spray cooling and pool boiling[4-11] as well as in air cooling[16] In all these cases (drop/spray cooling, pool boiling and forced air convection) it was reported the copper-plated nanofibers increased the heat transfer rate dramatically.

The authors of Ref. [18] prepared flower-like copper oxide nanostructures, which were used to enhance heat transfer in pool boiling Due to the high surface-to-volume ratio of these nanostructures, capillary wicking occurred, which in turn, increased the critical heat flux by 58%. Different designs and dimensions of microchannel heat sinks have also been extensively studied[19, 20], as well as it was demonstrated that microchannel flows of suspensions of carbon nanotubes filled with phase change materials could be beneficial as heat sinks[21]. The effect of particle-laden water on critical heat flux in pool boiling was demonstrated[22]. It was shown that inclusion of titania and alumina nanoparticles enhanced the critical heat flux as compared to that of pure water.

The above-mentioned references reveal that nano-texturing is useful for enhancing heat transfer rate. Herein, we employ various nanomaterials (thorny-devil nanofibers, reduced graphene-oxide (rGO), and silver nanowires) which yield different nano-textured surfaces and thus different heat transfer patterns in forced convection of water over such surfaces. All of these nanomaterials possess high surface-to-volume ratios, and being deposited on a surface create a “fluffy” layer which facilitates enhanced heat transfer.

2. Experimental

2.1 Water cooling system

The experimental setup of the heat sink system used in the present study is shown in **Figure 1**. The loop consists of a thermostat (Lab. Companion, RW-0525G), heat-sink (or often called as "cold plate"), data acquisition unit (MV-1000, YOKOGAWA, Japan), and power supply. Working liquid at 15±1 ºC was pumped from the thermostat though the heat-sink inlet and then from its outlet to the thermostat.

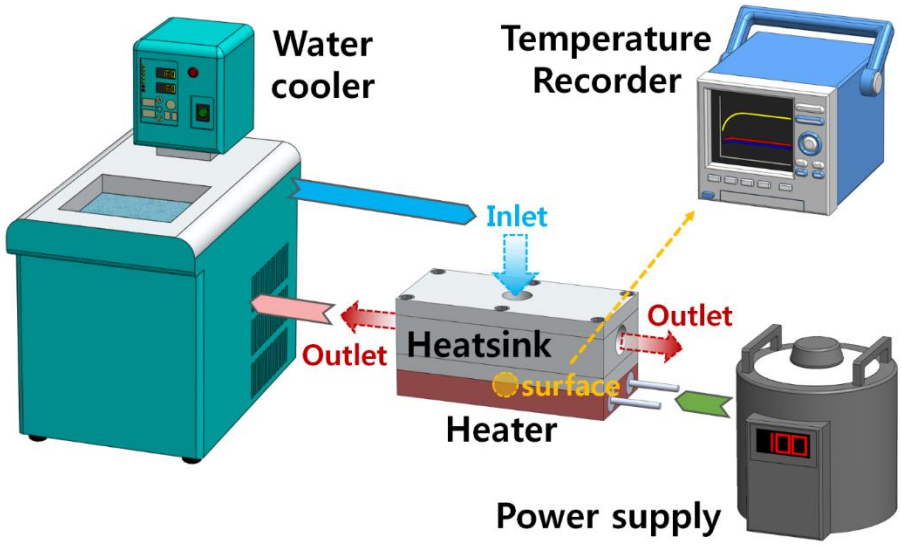

Figure 1. Schematics of the heat-sink system. Cold water is supplied into the inlet of the heat-sink, which incorporates nano-textured surfaces. The heater is cooled therefore and the heat transfer from the nano-textured surface of the heater to cold water takes place. A thermocouple is embedded at the bottom of the heater surface to monitor its temperature. The heated water exits back to the water cooler/chiller and the cold inlet temperature is reset.

The flow rate (3.1-9.1 mL/s) of the working fluid (water) was measured with an accuracy of ±1%. The temperature of the heat-sink was measured, at the bottom side, by T-type thermocouples (probe size = 1.0 × 150 mm), with an accuracy of ±0.1 $^{\circ}$C. The data were collected by the data acquisition unit.

The test module consisted of a top cover, rubber sealing, middle frame, copper plate, bottom cover, and a heater as illustrated in **Figure 2(a)**. Top and bottom cover are bolted with the middle frame using Hex Socket-Head Cap Screw. A detail schematic of the heat sink, thermocouple, copper substrate, and heater (the bottom copper plate decorated with sprayed nano-textured material) are shown in **Figure 2(b)**. The heat sink was fabricated from stainless-steel. The top cover of the heat sink was 0.5 cm in thickness, 6.5 cm wide and 3.0 cm deep. Water flow was passing through the channel cross-section of 1 cm $\times$ 1 cm as shown in **Figure 2(a)**. Nano-textured materials were sprayed onto the copper bottom and were located on its side facing the impinging water flux.

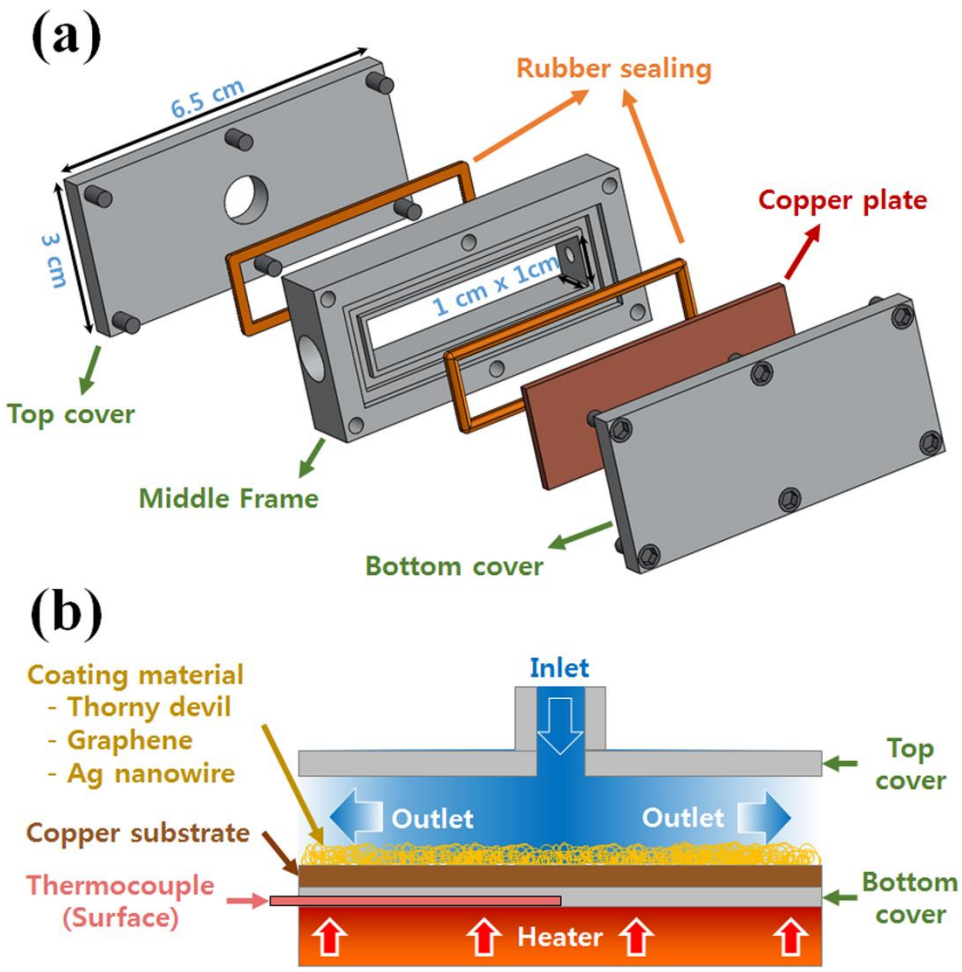

Figure 2. Detailed schematics of the test module. (a) Assembly of the heat sink. (b) The heat sink attached to the heater. Water enters the heat-sink through the top cover and exits both sideways. The copper substrate is decorated with either thorny-devil copper oxide nanofibers, or rGO, or silver nanowires. Heat is provided from the bottom and temperature is measured in the middle at the center of the impinging water flux.

2.2 Fabrication of nano-textured surfaces

2.2.1 Copper oxide nanofibers

The electrospun nanofibers was prepared from 6 wt % of polyacrylonitrile (PAN, $(C_3H_3N)_n$; M_w = 150 kDa; Sigma-Aldrich) in *N*,*N*-Dimethylformamide (DMF, $HCON(CH_3)_2$; anhydrous 99.8%; Sigma-Aldrich), while stirring by magnetic stirrer for 24 h at room temperature. To prepare the electroplating solution, sulfuric acid (10 g, H_2SO_4; 97%; Matsunoen Chemicals Ltd.), hydrochloric acid (1 g, HCl; 35%; Duksan Chemical), copper(II) sulfate (32 g, $CuSO_4$; 99.99%; Sigma-Aldrich), and formaldehyde solution (20 g, HCHO; 35%; Samchun Chemicals) were mixed with 200 mL of deionized (DI) water. Sulfuric acid increased solution conductivity to enhance of the electroplating process.

The PAN 6 wt % solution was supplied by a syringe pump (KDS LEGATO 100) at the flow rate of Q = 150 μL/h to a needle with the inner and outer diameters of 0.25 and 0.52 mm, respectively (EFD 25 gauge). The needle was attached to a DC source (Glassman High Voltage Inc., EL40P1). The applied voltage was in the 5 − 6 kV range. The nozzle-to-substrate distance was 10 cm. The PAN nanofibers were electrospun onto a copper substrate and subsequently copper-plated on top of it, thus creating a nano-textured surface.

2.2.2 Reduced graphene oxide

To form another type of nano-textured surface, the rGO solution consisting of rGO flakes (N006-P, Angstron Materials, USA) dispersed in dimethylformamide (DMF) was purchased from Duksan Chemical, Korea, used as dispersant. More detail on the rGO flakes used can be

found in **Table 1**. The rGO solution atomized in the Laval nozzle and formed supersonic kinetic spray as reported in our previous paper[23]. The copper substrate was located at 60 mm from the Laval nozzle exit. The nozzle exit was installed on a maneuvering stage that traversed the 50 mm length. The moving nozzle could, in principle, traverse the length of any fixed substrate that might be required to cover a larger coating area. The atomized rGO suspension droplets moved through open air at room temperature until they were deposited onto the copper substrate and formed nano-textured rGO coatings.

Table 1. Properties of rGO flake

Property [unit]	Typical value
Average *Z* dimension [nm]	10 – 20
Average *X* and *Y* dimensions [μm]	≤ 5
Surface area [m^2/g]	15
Density [g/cm^3]	2.2

2.2.3 Silver nanowires

Silver nanowires (AgNW, 0.15 wt%) dispersed in Isopropyl alcohol (IPA) were purchased from AIDEN Co. The nanowires possessed an average diameter and length of 20 nm and 15 μm, respectively. A transparent and homogeneous suspension of AgNWs was stirred with magnetic bar and subsequently aged for 1 h. Then, AgNWs were spin-coated on a pre-cleaned copper substrate (53 mm × 20 mm). A 0.5 mL drop of AgNW suspension was dripped onto a copper substrate, which was spun for 30 s at 4,000 rpm using a spin coater. Then, the substrate

was pre-annealed at 250 °C on a hotplate. This process was repeated eight times to form a copper surface with AgNW nano-textured structure. Finally, such surfaces were annealed in air using a two-step process in a closed furnace; at the first step, the surfaces were annealed for 15 min at 300 °C to remove the IPA (isopropyl alcohol) effectively, and then further annealed for 60 min at 500 °C enhance AgNW adhesion to the copper substrate.

2.2.4 Vortex generators

Two copper wires of 1 mm in diameter were attached to the copper substrate by soldering to serve as macroscopic vortex generators and to compare and discriminate their effect on heat transfer from that of nano-textured structures located at the substrate surface in the other experiments in this work.

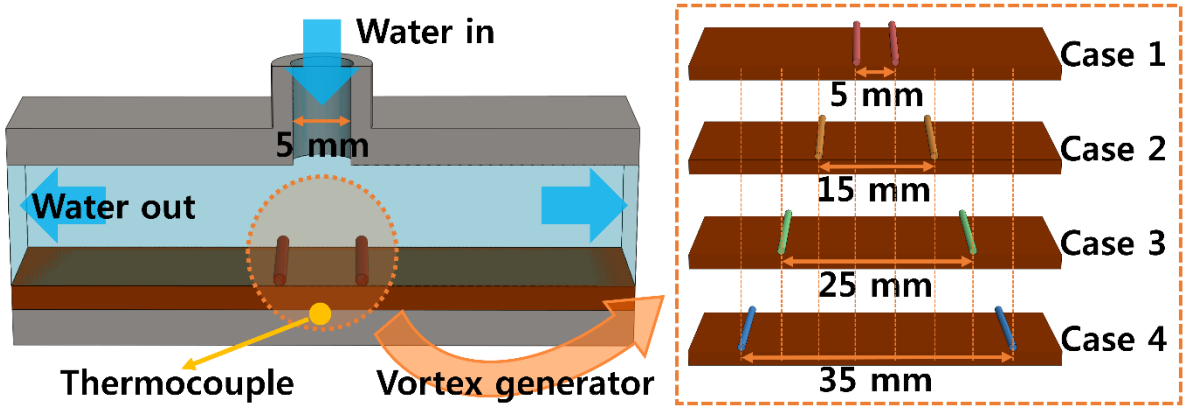

Figure 3. Schematic of the arrangement of the copper wire vortex generators attached to a copper substrate. The distance between the two vortex generator wires was varied according to the inset on the right-hand side and denoted as Cases 1, 2, 3, and 4. The impinging water flux is directly injected onto the substrate supporting vortex generators. The spreading water flow produces the von Karman vortex street, while passing over the vortex generators and the heat transfer might be enhanced accordingly.

With the volumetric flow rates of water in the 3.1 cm^3/s - 9.1 cm^3/s range through a cross-section of 1 cm^2, the average flow velocity V is in the 3.1 cm/s - 9.1 cm/s range. Accordingly, the Reynolds number for the channel flow Re_{ch} = 310 to 910, which shows that the flow is practically laminar. In addition, the Reynolds number of a wire vortex generator of d = 0.1 cm, Re_d = 31 to 91. This is the range of the Reynolds numbers where a well-developed von Karman vortex street is formed [24], which is prone to intensify the heat transfer in the wire wake. This action of the wires is similar to the action of wire vortex generators which generate fully developed turbulence in the wake. Therefore, the wires are conditionally called vortex generators in the present case as well. The location of the vortex generators was varied in the 5 – 35 mm range to control the enhancement the heat transfer by the vortices in the von Karman vortex street (cf. **Figure 3**).

2.3 Characterization

Thorny devil nanofibers, graphene, and AgNWs nano-textured surfaces were characterized using a high resolution scanning electron microscope (SEM, Hitachi S-5000, Japan). A non-contact mode atomic force microscope (AFM; XE-100, Park Systems Corp., Suwon, Korea) was also used to examine the surface morphology, surface area, and roughness of nano-textured substrates. A data acquisition unit was used to measure the surface temperature of the heat sink.

3. Results and Discussion

3.1 Surface morphology

Figure 4 shows the SEM images of the bare and nano-textured surfaces (the latter with thorny devil nanofibers, rGO flakes and AgNWs). The first and second row images show the surfaces before and after their use in water cooling. There is no discernable change in

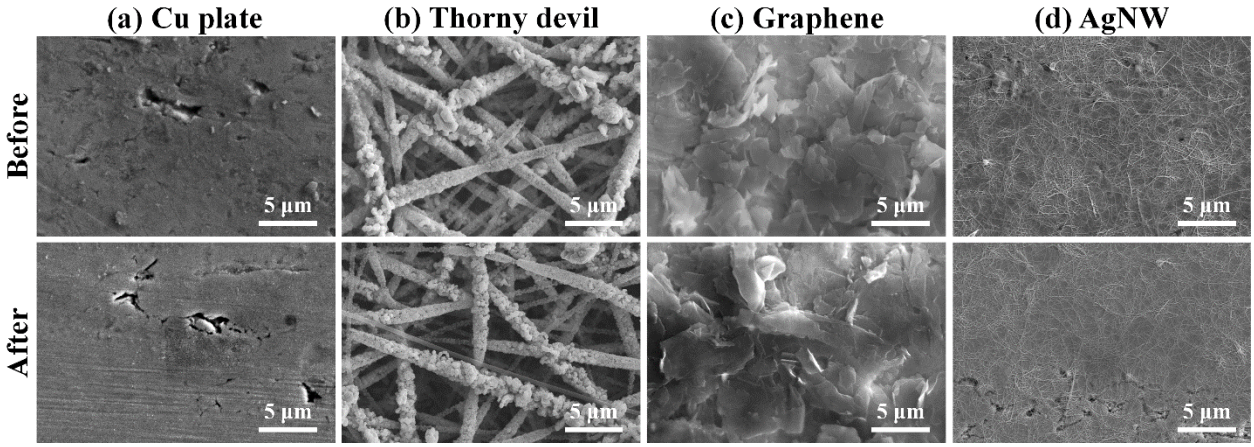

Figure 4. SEM image of nano-textured substrates. (a) Bare Cu plate. (b) Copper substrate covered with thorny devil nanovires. (c) Copper substrate covered with rGO graphene. (d) Copper substrate covered with AgNWs. The row marked "Before" shows the surfaces before they were subjected to water flow, while to row marked "After" shows the surfaces after a prolong exposure to water flow.

surface morphology between the one observed before and the one observed after more than 10 cycles of use. Each cycle lasted for about 60 min. The impinging water from the inlet did not result in any damage in the original nano-textured surface. Thus, the structures formed in this work are stable and remains intact and robust, as well as adherent to the underlying substrate. These nanostructures are expected to provide an enhances surface area for heat transfer as well

as to probably add a moderate extra flow mixing [16], which could also affect heat transfer, the effect which is explored below.

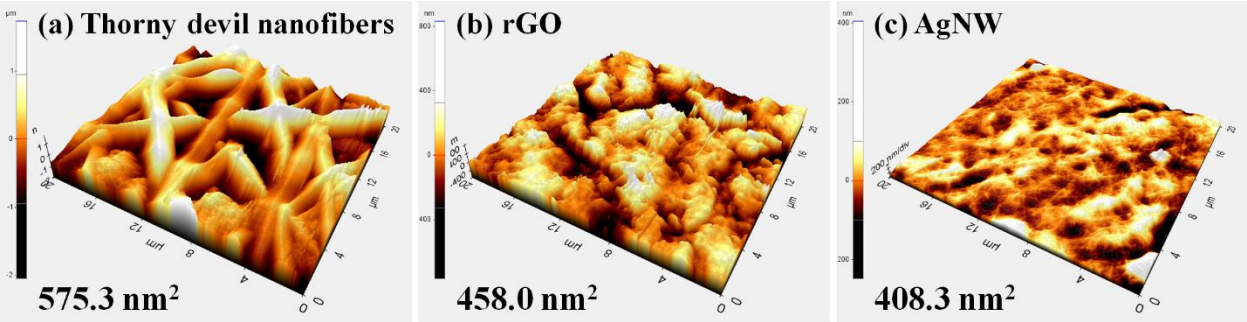

Figure 5. AFM images of the nano-textured copper substrates. (a) Thorny devil nanofibers, (b) rGO, and (c) AgNW-coated substrates. The surface areas of the nano-textured substrates (with the same projected areas) are given in the lower right corner. The scan substrate area was 20 × 20 nm^2.

The surface topographies of the fabricated nano-textured surfaces were characterized by AFM. The 3D AFM surface morphologies of electroplated thorny devil nanofibers, spray-coated rGO and spin-coated AgNWs on copper substrates are shown in **Figure 5.** The AFM observations indicate a sharp-peak topography of the thorny-devil nanofibers and the corresponding surface area was estimated as 575.3 nm^2. The surface area of the rGO and AgNW –coated substrates were lower, 458 and 408.3 nm^2, respectively. The effect of the enhanced surface area provided by nano-textures on the heat transfer rate is discussed below.

3.2 Heat transfer enhancement on nano-textured surfaces

Figure 6 compares the temperature histories recorded on different surfaces. The data was collected up to 1 h, so that steady-state would be achieved in all the cases. In each case, the experiments were conducted in triplicate to produce statistically sound data. The flow rate of $\dot{m}$ = 3.1 ×10^{-3} kg/s was fixed.

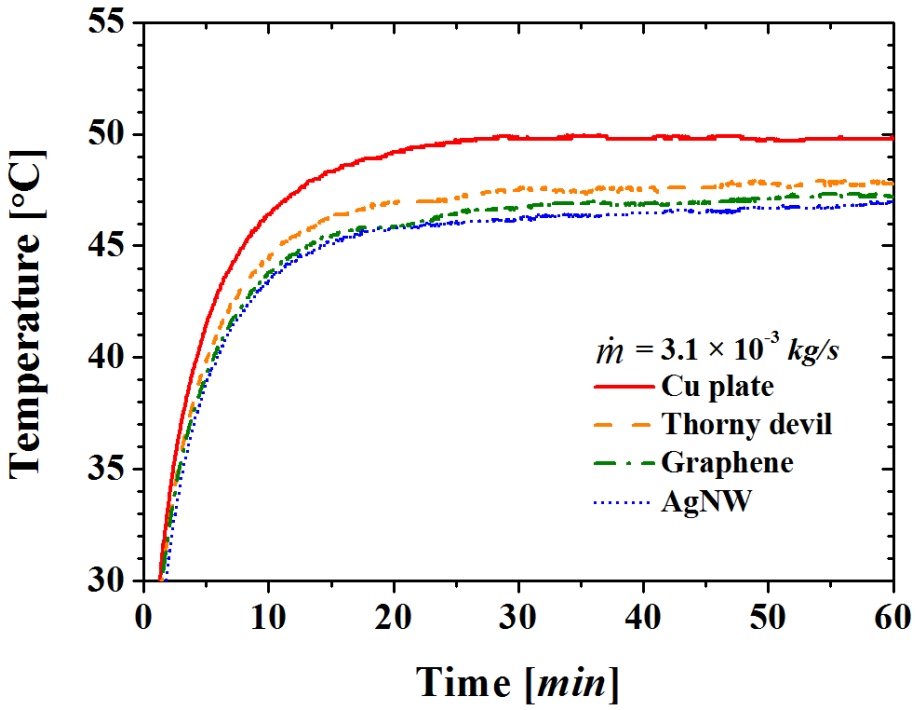

Figure 6. Temperature measured at the center of the substrates connected to the heater. The bare Cu surface reveals the highest steady-state temperature, i.e. the lowest heat transfer rate. On the other hand, the nano-textured surfaces progressively reduce the steady-state surface temperature, i.e. enhance heat transfer. The flow rate was fixed at $\dot{m}$ = 3.1 ×10^{-3} kg/s. The error bars of the temperature measurement are ±0.1°C.

The solid line for the bare copper substrate in **Figure 6** reveals the highest steady-state temperature because in the absence of nano-texture the surface area is minimal (400 nm^2, cf. **Figure 5**). Apparently, all of the nano-textured surfaces contributed to the steady-state temperature reduction in the 2 – 3 $^{\circ}$C range. AgNWs (with the 8 subsequent spin-coating depositions) yielded the lowest steady-state temperature. The rGO film yielded the second lowest temperature and the thorny-devil nanofibers resulted in the highest steady-state temperature among all of the nano-textured surfaces. It should be emphasized that according to **Figure 5**, the AgNW-coated surface possesses the lowest surface area compared to those of the graphene-coated and nanofiber-coated surfaces, and yet results in the lowest temperature. **Figure 4** shows that AgNWs possess smaller scales compared to the other nano-textured structures deposited on copper surface. One can speculate that AgNWs might be flexible under the drag imposed by water flow and thus facilitate local mixing and heat transfer.

3.3 Effect of flow rate on the heat transfer on nano-textured AgNW surface

Convective heat transfer is enhanced at a higher flow rate ("wind chill"). For the nano-textured AgNW-coated surfaces this is illustrated by the data in **Figure 7**. The highest flow rate yields the lowest temperature. **Table 2** lists the temperature differences measured between the outlet and inlet of the heat sink.

The inlet water temperature was about 16.5 $^{\circ}$C. The outlet water temperatures were higher due to heat removed from the substrate. It should be emphasized that even though the temperature difference $\Delta T = T_{out} - T_{in}$ decreases as the mass flowrate $\dot{m}$ increases, the overall heat removal rate from the heater $\dot{Q} = \dot{m}\, c_p \Delta T$ increases with $\dot{m}$, which determines lower heater

temperatures corresponding to higher values of $\dot{m}$ in **Figure 7**; c_p is the specific heat of water. The values of $\dot{Q}$ are listed in **Table 2.**

Table 2. Effect of flow rate on the difference between the outlet and inlet temperatures across the heat-sink and the heat removal rate.

$\dot{m}$ [kg/s]	$\Delta T = T_{out} - T_{in}$ [°C]	$\dot{Q}$ [Watt]
3.1×10^{-3}	1.0	13.00
4.8×10^{-3}	0.9	18.11
9.1×10^{-3}	0.5	19.08

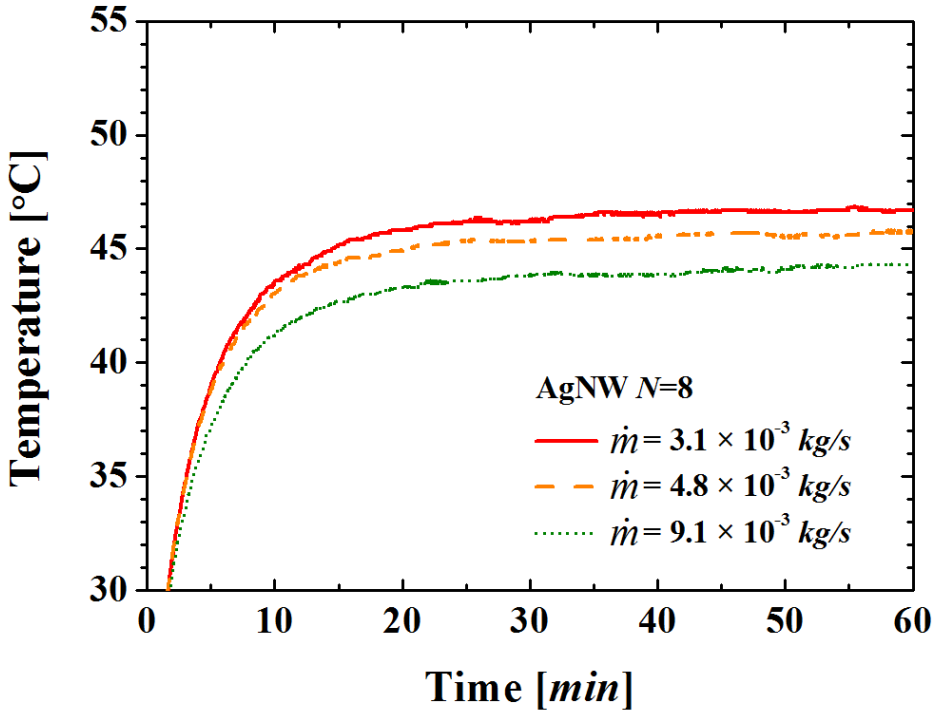

Figure 7. The effect of water flow rate on the substrate temperature. The nano-textured substrate was fabricated with AgNWs after *N* = 8 spin-coating depositions. The error bars of the temperature measurement are ±0.1 °C.

3.4 Effect of the AgNW amount

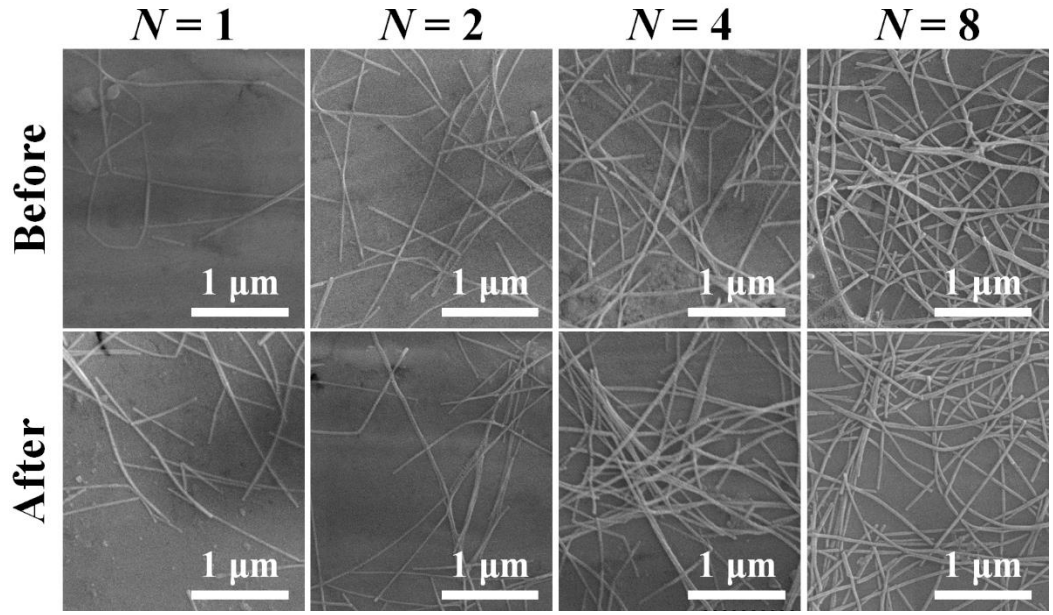

Figure 8. SEM image of various coatings of AgNW on Cu substrate achieved after *N* cycles of spin coating. The rows marked Before and After correspond to the coatings before and after they were subjected to water flux.

Parametric studies were conducted by varying the number of spin-coating deposition cycles (*N*) using silver nanowires. **Figure 8** shows the SEM images of the silver nanowires deposited on a copper substrate while varying *N*. The greater the number of spin coating cycles, the greater is the number of AgNWs deposited per unit area of substrate. The images compare the AgNW

morphology before and after they were subjected to water flux through the heat sink. The images were taken after 10 cycles (60 min each) of cooling. Because AgNWs were sintered at 200 °C after deposition, they were tightly bonded together and to the underlying copper substrate. These nanowires were not washed away by the impinging water flux entering through the inlet of the heat sink and spreading over its bottom. Ten random locations were observed, and it was confirmed that no discernable change in the nano-texture happened during the tests irrespective of the number N of spin-coating deposition cycles.

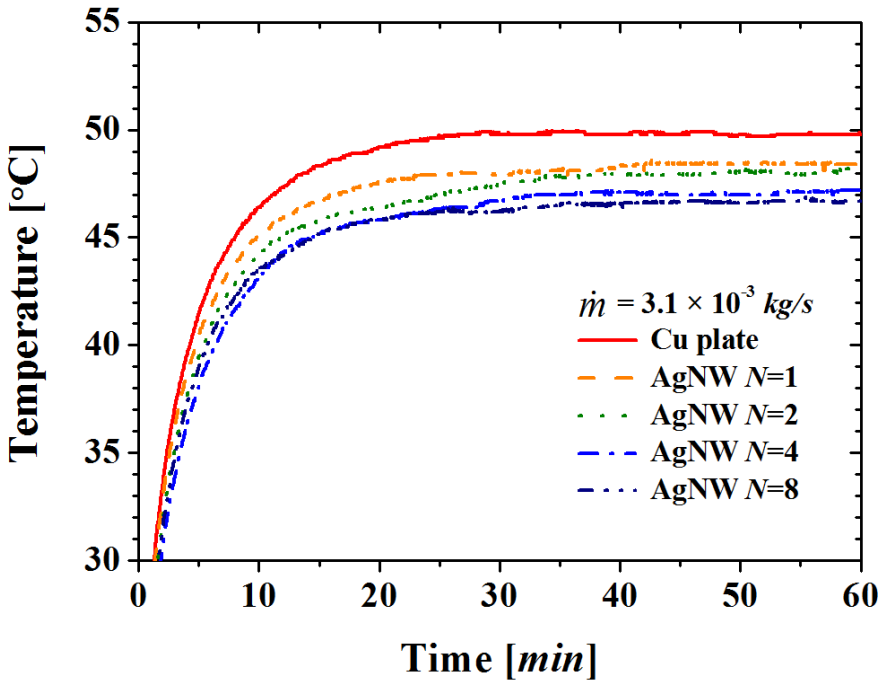

Figure 9. Heat-sink performance after *N* spin-coating cycles AgNWs deposition.

Figure 9 elucidates the effect of the number of AgNWs deposited on the substrate by varying the number of spin-coating cycles *N* on the temperature reduction at a fixed flow rate of $\dot{m}$ = 3.1 × 10^{-3} kg/s. The effect of *N* is recognizable only up to *N* = 4, which makes further

deposition cycles redundant. This relatively low flow rate was chosen to observe an apparent effect of *N* and to minimize the power consumption and the acoustic noise generated by a pump running at higher flow rates.

3.5 Effect of vortex generators in comparison to the nano-textured structures

The enhancement of the heat removal rate due to the presence of macroscopic vortex generators (wires) in addition to that of nano-textured structures was studied to discriminate an extra mixing effect of the latter (if any) from that of the surface area increase provided by nano-structures.

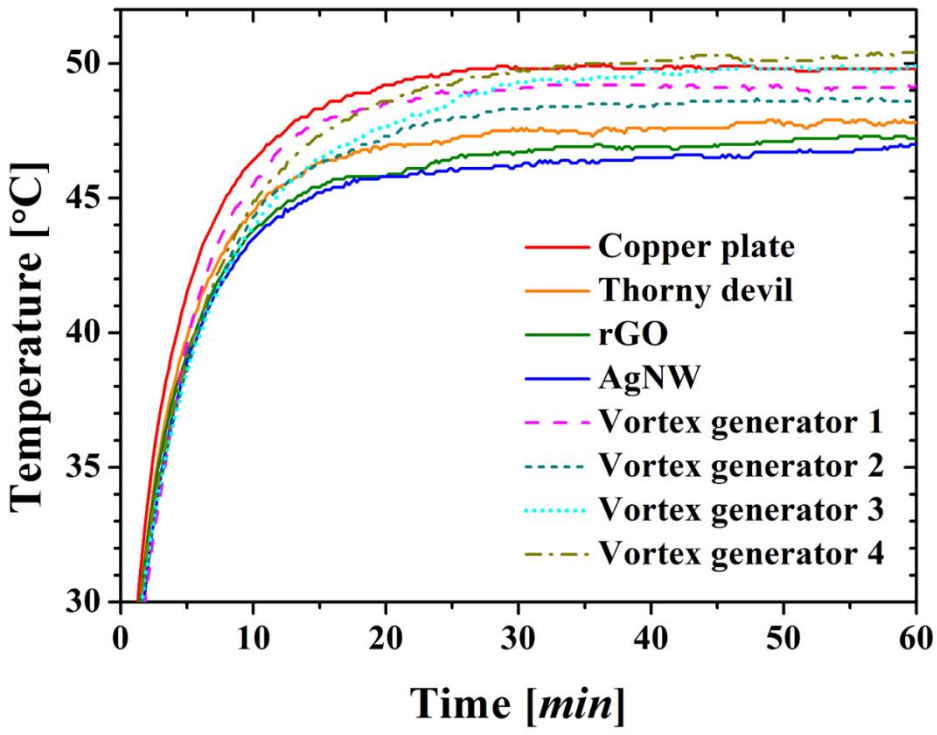

Figure 10. The effect of macroscopic vortex generators versus the effect of nano-textured structures. A fixed flow rate of $\dot{m}$ = 3.1 × 10^{-3} kg/s was used.

Figure 10 compares the bottom temperatures achieved in the presence of the macroscopic vortex generators located at different positions (cf. **Figure 3**) compared to that of the nano-textured surfaces discussed in the previous sections. It is remarkable to see that even though the extra mixing effect of the macroscopic wires is un-comparably stronger than that of the nano-structures, the latter reduced the bottom temperature much more. This makes it evident that an increased surface area associated with the nano-textured surfaces is surely the dominant factor in cooling enhancement on such surfaces, rather than the extra mixing effect. The extra mixing effect definitely facilitates heat transfer enhancement as **Figure 10** shows, however, the associated reduction of the bottom temperature is relatively small (see the cases for Vortex generators 1 and 2. On the other hand, when the vortex generator is located too farther away from the center, it has an adverse effect on cooling and even contributes to the temperature increase, as shown in **Figure 10** for Vortex generator 4. This is probably because flow separation before such a distant vortex generator happens which diminishes heat removal.

3.6 Heat transfer coefficient

The power supplied by the heater in steady-state regime when the difference between the outlet and inlet temperatures does not vary in time anymore, is fully removed by flowing water leaving the hot sink. Accordingly, $Q = \dot{m}\, c_p \Delta T$. Note that a potential heat loss from the heater to the surrounding air is negligibly small compared to that of water, since their thermal conductivity coefficients are incommensurate (the thermal conductivity of water is higher than the thermal conductivity of air by the factor of more than 20; in addition, the flowing water results in the

'chilling effect"). Then, the effective heat transfer coefficient h_{eff} based on the experimental results for Q listed in **Table 3** is found as [25,26]

$$h_{\text{eff}} = \frac{Q}{A(T_s - T_\infty)} \tag{1}$$

where T_s is the surface temperature, the estimated surface area is $A = 0.03 \times 0.065$ m^2, and the temperature of the inlet water is $T_\infty = 16.5$ °C.

On the other hand, the magnitude of Q can be evaluated from Fourier's law as

$$Q = \frac{kA}{\Delta x}(T_s - T_1) \tag{2}$$

where k is the thermal conductivity of copper, T_1 is the temperature value measured at the bottom of the copper substrate, and Δx is the thickness of the copper substrate (0.5 cm). Then, the surface temperature found from Eq. (2) reads

$$T_s = T_1 + Q\frac{\Delta x}{kA} \tag{3}$$

Table 3. Heat transfer coefficients.

$\dot{m}$ [kg/s]	h_{eff} (W/m^2·°C)

Cu plate		3.1×10^{-3}	163
Thorny devil		3.1×10^{-3}	203
Graphene		3.1×10^{-3}	207
AgNW	$N = 1$	3.1×10^{-3}	174
	$N = 2$	3.1×10^{-3}	179
	$N = 3$	3.1×10^{-3}	209
	$N = 8$	3.1×10^{-3}	221
	$N = 8$	4.8×10^{-3}	319
	$N = 8$	9.1×10^{-3}	353
vortex generator 1		3.1×10^{-3}	168
vortex generator 2		3.1×10^{-3}	175
vortex generator 3		3.1×10^{-3}	156
vortex generator 4		3.1×10^{-3}	146

Table 3 shows that the highest heat transfer coefficient was achieved with AgNWs at N=8. It should be emphasized that no appropriate correlations for the Nusselt number for heat sinks comparable to the previous one are available in the literature, as to our knowledge, since the well-known correlations for the impinging jets (cf. [26] are references therein) cannot be applied to the previous severely confined case. Therefore, the only way to elucidate the improvement of heat transfer due to the presence of nano-texture on the heat transfer surface is to compare the measured values for such surfaces in Table 3 with the one for the bare copper surface. Such a comparison shows that all nano-textured surfaces revealed a higher heat transfer coefficient than the bare copper surface, thus elucidating the enhancement achieved.

4. Conclusion

Nano-textured surfaces facilitate cooling which occurs in a heat sink with water through flow. The most significant cooling was achieved using nano-textured surface comprised of silver nanowires, then the nano-textured surface comprised of graphene oxide flakes, and then, the nano-textured surface comprised of electrospun copper-plated nanofibers. All these surfaces dramatically increase the surface area available for heat transfer. The heat transfer enhancement by macroscopic wires deposited on the surface to serve as vortex generators was much less pronounced, and sometimes even detrimental depending on the location of the vortex generators relative to the symmetry axis of the impinging water flow. This confirms the fact that the increase in the surface area, rather than the extra mixing of the flow, is the main mechanism of heat transfer enhancement on the nano-textured surfaces. However, the fact that of all nano-textured surfaces the best cooling effect was achieved with the one with the lowest surface area (silver nanowires) implies that AgNWs might be flexible under the drag imposed by water flow, which enhances local mixing and heat transfer. The fact that the nano-structure with a lower surface area than the other one provides the best cooling effect is non-trivial and shows that the generally invoked idea of just the increase in surface area can be intrinsically flawed and additional physical factors can be at play.

Acknowledgement

This work was supported by the Industrial Strategic Technology Development Program (10045221) funded by the Ministry of Knowledge Economy (MKE, Korea) and NRF-2013M3A6B1078879. This research was partially supported by the Commercializations Promotion Agency for R&D Outcomes (COMPA) funded by the Ministry of Science, ICT and Future Planning (MISP). S.S. Yoon expressed his thanks to the support made by King Saud University, Vice Deanship of Research Chairs

References

[1] R. Elnathan, M. Kwiat, F. Patolsky, N.H. Voelcker, Engineering Vertically Aligned Semiconductor Nanowire Arrays for Applications in the Life Sciences, Nano Today, 9(2) (2014) 172-196.

[2] M. Qu, J. Wu, G. Zhao, Y. Zhang, Nanostructured Surfaces, Coatings, and Films: Fabrication, Characterization, and Application, Journal of Nanomaterials, 2013 (2013) 1-2.

[3] Z.L. Wang, Zinc Oxide Nanostructures: Growth, Properties and Applications, J. Phys.: Condens. Matter, 16(25) (2004) R829-R858.

[4] R. Srikar, T. Gambaryan-Roisman, C. Steffes, P. Stephan, C. Tropea, A. Yarin, Nanofiber Coating of Surfaces for Intensification of Drop or Spray Impact Cooling, Int. J. Heat Mass Transfer, 52(25) (2009) 5814-5826.

[5] S. Sinha-Ray, Y. Zhang, A.L. Yarin, Thorny devil nanotextured fibers: the way to cooling rates on the order of 1 kW/cm^2, Langmuir, 27(1) (2010) 215-226.

[6] C.M. Weickgenannt, Y. Zhang, A.N. Lembach, I.V. Roisman, T. Gambaryan-Roisman, A.L. Yarin, C. Tropea, Nonisothermal Drop Impact and Evaporation on Polymer Nanofiber Mats, PhRvE, 83(3) (2011) 036305.

[7] C.M. Weickgenannt, Y. Zhang, S. Sinha-Ray, I.V. Roisman, T. Gambaryan-Roisman, C. Tropea, A.L. Yarin, Inverse-Leidenfrost Phenomenon on Nanofiber Mats on Hot Surfaces, PhRvE, 84(3) (2011) 036310.

[8] S. Sinha-Ray, A.L. Yarin, Drop Impact Cooling Enhancement on Nano-textured Surfaces. Part I: Theory and Results of the Ground (1g) Experiments, Int. J. Heat Mass Transfer, 70 (2014) 1095-1106.

[9] S. Sinha-Ray, S. Sinha-Ray, A.L. Yarin, C.M. Weickgenannt, J. Emmert, C. Tropea, Drop Impact Cooling Enhancement on Nano-textured Surfaces. Part II: Results of the Parabolic Flight

Experiments [zero gravity (0g) and supergravity (1.8 g)], Int. J. Heat Mass Transfer, 70 (2014) 1107-1114.

[10] S. Jun, S. Sinha-Ray, A.L. Yarin, Pool Boiling on Nano-textured Surfaces, Int. J. Heat Mass Transfer, 62 (2013) 99-111.

[11] R.P. Sahu, S. Sinha-Ray, S. Sinha-Ray, A.L. Yarin, Pool Boiling on Nano-textured Surfaces Comprised of Electrically-assisted Supersonically Solution-blown, Copper-plated Nanofibers: Experiments and Theory, Int. J. Heat Mass Transfer, 87 (2015) 521-535.

[12] R. Chen, M.-C. Lu, V. Srinivasan, Z. Wang, H.H. Cho, A. Majumdar, Nanowires for Enhanced Boiling Heat Transfer, Nano Lett., 9(2) (2009) 548-553.

[13] T.J. Hendricks, S. Krishnan, C. Choi, C.-H. Chang, B. Paul, Enhancement of Pool-boiling Heat Transfer using Nanostructured Surfaces on Aluminum and Copper, Int. J. Heat Mass Transfer, 53(15-16) (2010) 3357-3365.

[14] H.S. Ahn, H.J. Jo, S.H. Kang, M.H. Kim, Effect of Liquid Spreading due to Nano/Microstructures on the Critical Heat Flux During Pool Boiling, Appl. Phys. Lett., 98(7) (2011) 071908.

[15] J. Choi, M. Ha, Y. Lee, S. Graham, H. Kang, Thermal Management of High Density Power Servers using a Compact Two-phase Loop Cooling System, in: Semiconductor Thermal Measurement and Management Symposium (SEMI-THERM), 2013 29th Annual IEEE, IEEE, 2013, pp. 29-32.

[16] S. An, C. Lee, M. Liou, H.S. Jo, J.J. Park, A.L. Yarin, S.S. Yoon, Supersonically Blown Ultrathin Thorny Devil Nanofibers for Efficient Air Cooling, ACS Appl Mater Interfaces, 6(16) (2014) 13657-13666.

[17] T. Alam, P.S. Lee, C.R. Yap, Effects of Surface Roughness on Flow Boiling in Silicon Microgap Heat Sinks, Int. J. Heat Mass Transfer, 64 (2013) 28-41.

[18] Y. Im, C. Dietz, S.S. Lee, Y. Joshi, Flower-Like CuO Nanostructures for Enhanced Boiling, Nanoscale and Microscale Thermophysical Engineering, 16(3) (2012) 145-153.

[19] A.M. Adham, N. Mohd-Ghazali, R. Ahmad, Thermal and Hydrodynamic Analysis of Microchannel Heat Sinks: A Review, Renew. Sust. Energ. Rev., 21 (2013) 614-622.

[20] S. Saisorn, S. Wongwises, A Critical Review of Recent Investigations on Flow Pattern and Heat Transfer during Flow Boiling in Micro-Channels, Frontiers in Heat and Mass Transfer, 3(1) (2012).

[21] S. Sinha-Ray, S. Sinha-Ray, H. Sriram, A.L. Yarin, Flow of Suspensions of Carbon Nanotubes Carrying Phase Change Materials Through Microchannels and Heat Transfer Enhancement, LChip, 14(3) (2014) 494-508.

[22] H. Kim, J. Kim, M.H. Kim, Effect of Nanoparticles on CHF Enhancement in Pool Boiling of Nano-fluids, Int. J. Heat Mass Transfer, 49(25) (2006) 5070-5074.

[23] D.Y. Kim, S. Sinha-Ray, J.J. Park, J.G. Lee, Y.H. Cha, S.H. Bae, J.H. Ahn, Y.C. Jung, S.M. Kim, A.L. Yarin, Self-Healing Reduced Graphene Oxide Films by Supersonic Kinetic Spraying, Adv. Funct. Mater., 24(31) (2014) 4986-4995.

[24] M. van Dyke. *An Album of Fluid Motion*. The Parabolic Press, Stanford, 1982.

[25] J. Holman, *Heat Transfer*, 10th ed.; McGraw-Hill: Boston, 2010.

[26] S. An, C. Lee, M. Liou, H. S. Jo, J.-J. Park, A. L. Yarin, S. S. Yoon. Supersonically Blown Ultra-thin Thorny Devil Nanofibers for Efficient Air Cooling. ACS Applied Materials & Interfaces, 6 (2014), 13657-13666.